The 3D geometry of reflection nebulae IC 59 and IC 63 with their illuminating star gamma Cas

Jacob M. Eiermann [1]★ Miranda Caputo [2] Thomas S.-Y. Lai [3] and Adolf N. Witt [2]

[1]*Department of Physics & Astronomy, University of Georgia, Sanford Drive, Athens, GA 30602, USA*
[2]*Ritter Astrophysical Research Center, University of Toledo, Toledo, OH 43606, USA*
[3]*IPAC, California Institute of Technology, 1200 E. California Blvd., Pasadena, CA 91125, USA*

ABSTRACT

The early-type star gamma Cas illuminates the reflection nebulae IC 59 and IC 63, creating two photodissociation regions (PDRs). Uncertainties about the distances to the nebulae and the resulting uncertainty about the density of the radiation fields incident on their surfaces have hampered the study of these PDRs during the past three decades. We employed far-ultraviolet (UV) – optical nebula – star colour differences of dust-scattered light to infer the locations of the nebulae relative to the plane of the sky containing gamma Cas, finding IC 63 to be positioned behind the star and IC 59 in front of the star. To obtain the linear distances of the nebulae relative to gamma Cas, we fit far-infrared archival *Herschel* flux data for IC 59 and IC 63 with modified blackbody curves and relate the resulting dust temperatures with the luminosity of gamma Cas, yielding approximate distances of 4.15 pc for IC 59 and 2.3 pc for IC 63. With these distances, using updated far-UV flux data in the 6–13.6 eV range for gamma Cas with two recent determinations of the interstellar extinction for gamma Cas, we estimate that the far-UV radiation density at the surface of IC 63 takes on values of $G_0 = 58$ or $G_0 = 38$ with respective values for $E(B - V)$ for gamma Cas of 0.08 and 0.04 mag. This is a substantial reduction from the range $150 \leq G_0 \leq 650$ used for IC 63 during the past three decades. The corresponding, even lower new values for IC 59 are $G_0 = 18$ and $G_0 = 12$.

Key words: scattering – methods: data analysis – ISM: clouds – HII regions – planetary nebulae: general.

1 INTRODUCTION

IC 59 and IC 63 are two reflection/emission nebulae that are externally illuminated by the bright B0.5IVpe star gamma Cas (Fig. 1). Sculpted by the UV radiation from gamma Cas, the nebulae appear as cometary neutral globules in a larger cavity of ionized gas surrounding the star (Chen et al. 2021), the H II region Sh2-185 (Blouin et al. 1997). Their relative proximity to Earth [$d = (168 \pm 4)$ pc; van Leeuwen (2007)] makes them ideal laboratories for studying the interaction of intense stellar UV radiation with molecules and dust, i.e. where models for photodissociation regions (PDRs) can be tested with the highest spatial resolution under conditions, where the PDR stratification can be clearly seen.

IC 63, the brighter of the two, has been the object of more extensive observation and study. It was this nebula where UV fluorescence emission of molecular hydrogen was first observed outside the Solar system (Sternberg 1989; Witt et al. 1989; Hurwitz et al. 1998; France et al. 2005). This discovery was followed in rapid succession by numerous other investigations at longer wavelengths directed at IC 63 as well as IC 59, with a focus on the physics and chemistry probed by a diverse array of molecules with their emission mechanisms (Jansen, van Dishoeck & Black 1994; Jansen et al. 1995, 1996; Blouin et al. 1997; Habart et al. 2004; France et al. 2005; Karr, Noriega-Crespo & Martin 2005; Thi et al. 2009; Fleming et al. 2010; Miao et al. 2010;

Andersson et al. 2013; Lai, Witt & Crawford 2017; Soam et al. 2017; Andrews et al. 2018; Van De Putte et al. 2020; Kaplan et al. 2021; Soam et al. 2021; Schirmer et al. 2022; Bonne et al. 2023; Caputo et al. 2023).

A persistent problem facing most of these investigations arose from the fact that the spatial distance from gamma Cas to the two nebulae was highly uncertain. The analysis of the data in PDR studies requires information about the density of the stellar UV radiation field incident on the nebulae. Lacking information about the positions of the nebulae along their respective lines of sight, most studies assumed that the nebulae were situated in the plane of the sky that contains gamma Cas, i.e. that the angular offsets from the star at the star's distance determined the physical distances. With the currently accepted distance to gamma Cas of (168 ± 4) pc, this offset distance amounts to about 1.0 pc in the case of IC 63 and 1.2 pc for IC 59. This resulted in the frequently used assumption that the UV radiation flux in the energy range 6–13.6 eV incident on the face of IC 63 amounts to about $G_0 = 650$ Draine units (Jansen, van Dishoeck & Black 1994), where one Draine unit is 2.7 x 10^{-3} erg s^{-1} cm^{-2} (Draine 1978), or about 1100 Habing (1968) units.

Jansen et al. (1995) was first in considering possible geometries where IC 63 was located behind gamma Cas, with the line toward IC 63 forming an angle of $30°$ with the plane of the sky at the location of gamma Cas. This would increase the distance to IC 63 to about 1.15 pc. This suggestion was pursued further by Andersson et al. (2013), who found that the angular offset between linear streaming features seen in maps of the 1–0 S(1) emission of H$_2$ and
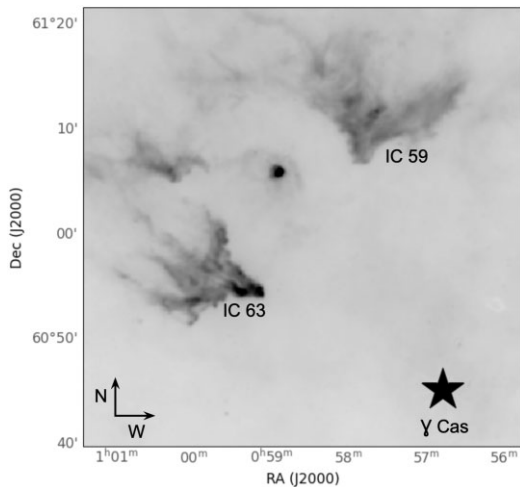
★ E-mail: eiermannj7@gmail.com

Figure 1. *WISE* Band 3 (12 μm) cutout of region containing gamma Cas with IC 59 and IC 63.

the direction of the incident radiation suggested instead an angle of 68° with the plane of the sky, placing IC 63 further behind. The linear distance from gamma Cas to IC 63 in this instance is about 2.7 pc. Analysing available data from the *Spitzer* and *Herschel* programmes, Andrews et al. (2018) concluded that the tips of IC 63 and IC 59 were, respectively, about three and five times farther away from gamma Cas than their projected angular offset distances, but with no indication as to the location of the nebulae relative to the plane of the sky containing gamma Cas. They recommended $G_0 = 150$ for IC 63 and $G_0 = 25$ for IC 59. Most recently, Caputo et al. (2023), from a study of [C II] kinematics in both nebulae, concluded that IC 63 is located behind the plane of the sky containing gamma Cas, at about 2 pc from gamma Cas, whereas IC 59 is placed in front of this plane at about 4.5 pc from gamma Cas, being irradiated at an angle of about 70°.

In this work, we used the observed surface brightness of dust-scattered light at optical and UV wavelengths and corresponding measurements of the flux from gamma Cas at Earth to determine the nebula–star colour differences for IC 63 and IC 59. Such colour differences are sensitive to changes in the effective scattering angle, because the scattering phase function of interstellar dust is strongly forward-throwing at UV-optical wavelengths, with the phase function asymmetry increasing toward shorter wavelengths (Witt 1985; Draine 2003; Baes, Camps & Kapoor 2022). Previously observed colour differences as a function of offset distance in the Merope nebula have demonstrated the magnitude and direction of this effect (Andriesse, Piersma & Witt 1977; Witt 1977). Thus, colour-difference measurements in IC 59 and IC 63 are useful in determining the locations of the nebulae along their lines of sight relative to gamma Cas. Additionally, we have used archival far-infrared (IR) *Herschel* data covering the 70–500 μm wavelength range to estimate the temperatures of large grains in equilibrium with the radiation field of gamma Cas. With information about the star's bolometric luminosity and assuming that large grains (approximate size range 100–1000 nm) are in equilibrium with the radiation field of gamma Cas, these temperatures yield estimates of the radial distance of the nebulae from gamma Cas, independent of direction. Further constraints on the ratio of these two distances come from measurements of the maximum intensities of extended red emission (ERE; Lai, Witt & Crawford 2017) in both nebulae. The ERE appears as an isotropic emission in the 5400–8500 Å wavelength range in many interstellar environments containing interstellar dust and far-

ultraviolet (far-UV) photons (Witt & Lai 2020). The ERE intensity has been shown to correlate with the density of the prevailing far-UV (10.5–13.6 eV) radiation field (Smith & Witt 2002; Witt et al. 2006) and can therefore be employed to estimate the density of such fields. Finally, we used the estimated linear distances from gamma Cas to the two nebulae, together with far-UV *International Union Explorer (IUE)* and *Far Ultraviolet Spectroscopic Explorer (FUSE)* spectra and existing constraints on the interstellar reddening of gamma Cas, to calculate the most likely UV radiation densities at the faces of IC 59 and IC 63.

We record the sources of our data in Section 2, followed by the analysis of the different data sets in Section 3. In Section 4, we discuss the limitations and uncertainties of our results arising from various assumptions made in the analysis, followed by a set of conclusions in Section 5.

2 DATA

2.1 Distance and luminosity of gamma Cas

We adopted the distance of (168 ± 4) pc for gamma Cas (van Leeuwen 2007), which is a reduction from the original Hipparcos distance of (188 ± 20) pc (Perryman et al. 1997), resulting from the corrections for systematic errors present in the original catalog. Most earlier investigations of the gamma Cas/IC 63/IC 59 system have assumed distances in the 230 pc (Jansen, van Dishoeck & Black 1994) to 190 pc (Caputo et al. 2023) range.

Setting aside the evidence for its long-term and cyclical variability (Henry & Smith 2012, and references therein), Sigut & Jones (2007) adopted the value $L_\star = 34\,000$ L$_\odot$ for the present luminosity of gamma Cas, with an assumed distance $d = 188$ pc. For our adopted distance of $d = 168$ pc, this reduces to $L_\star = 27\,150$ L$_\odot$, which we will use in our subsequent calculations.

2.2 Interstellar extinction

Gamma Cas is the well-studied prototype of classical Be stars. The colour excess $E(B - V)$ of Be stars is in part the result of free–free emission of their circumstellar discs affecting their V-magnitudes and is, therefore, not a suitable basis for estimating the interstellar extinction for such stars (Schild 1983). Nonetheless, interstellar absorption features such as the 2175 Å absorption band and diffuse interstellar bands (DIBs) that closely correlate with interstellar reddening have led to recent estimates of the interstellar reddening for gamma Cas. These values are $E(B - V) = (0.08 \pm 0.007)$ mag, based on the equivalent widths of the DIBs at 5780 and 5797 Å (Nikolov et al. 2017), and $E(B - V) = 0.04^{+0.03}_{-0.02}$ mag (Klement et al. 2017), arrived at by cancelling the 2175 Å band absorption in the ultraviolet Spectral Energy Distrbution (SED) of gamma Cas with an average galactic extinction curve of Cardelli, Clayton & Mathis (1989), hereafter referred to as CCM, with a ratio of total-to-selective extinction $R_V = 3.1$. We, therefore, adopt these reddening values as limiting values, and we further assume that the extension of the extinction curve into the UV follows a CCM curve with $R_V = 3.1$. Furthermore, we will assume that the light originating from IC 59, IC 63, and gamma Cas is subjected to the same amount of foreground interstellar extinction.

2.3 Surface brightness data for IC 59 and IC 63

We acquired low-resolution, large-aperture (10 arcmin x 20 arcmin) *IUE* spectra of IC 59 and IC 63 from the *Mikulski Archive for Space*

Table 1. Ultraviolet surface brightness measurements from *IUE* spectra.

		Position		Wavelength	Surface brightness
Object name	*IUE* Spec file ID	R.A.(2000.0)	DEC(2000.0)	(Å)	(erg cm^{-2} s^{-1} Å^{-1} sr^{-1})
IC 63	LWP17444	00:59:01.365	+60:53:17.56	2600–2800	(1.13 ± 0.12)E-06
IC 63	SWP33989	00:59:01.365	+60:53:17.56	1750–1900	(2.11 ± 0.35)E-06
IC 59	LWP17252	00:57:14.476	+61:07:28.34	2600–2800	(7.42 ± 1.80)E-07
IC 59	SWP38087	00:57:14.476	+61:07:28.34	1750–1900	(1.81 ± 0.43)E-06

Table 2. Measured $\log(S/F^{\star})$ in units of [sr^{-1}].

	Position					
Object name	R.A.(2000.0)	DEC(2000.0)	$\log(S/F^{\star})_{1825}$	$\log(S/F^{\star})_{2700}$	$\log(S/F^{\star})_B$	$\log(S/F^{\star})_G$
IC 63	00:59:01.365	+60:53:17.56	2.46 ± 0.03	2.55 ± 0.06	2.87 ± 0.02	2.99 ± 0.01
IC 59	00:57:14.476	+61:07:28.34	2.39 ± 0.07	2.36 ± 0.07	2.40 ± 0.02	2.45 ± 0.01

Telescopes (MAST). There are two spectra associated with IC 59 that were taken at different positions (RA: 00:57:42.431, DEC: +61:04:59.89 and RA: 00:57:14.476, DEC: +61:07:28.34) within that nebula; we selected the second, brighter of the two for its more favourable signal-to-noise (S/N) ratio. For both IC 59 and IC 63, we integrated the nebular scattered-light fluxes in two bands, 2600–2800 and 1750–1900 Å. We chose these bands for their relatively high S/N ratio in the first case, and in the second instance, to avoid contamination by the far-UV fluorescence of H_2 that dominates the spectrum of IC 63 at wavelengths shorter than 1650 Å (Witt et al. 1989). We note that fluxes observed from extended sources, such as IC 59 and IC 63, depend on the limited solid angles of the apertures of the *IUE* spectrometers, projected on to the plane of the sky. Therefore, the nebular surface brightness becomes a more meaningful physical measure of the nebular brightness. To convert the fluxes, expressed in units of (erg cm^{-2} s^{-1} Å^{-1}) into surface brightness units of (erg cm^{-2} s^{-1} Å^{-1} sr^{-1}), we adopted the following solid angles subtended by the large *IUE* apertures: SWLA $= 5.03$ x 10^{-9} sr for the short-wavelength, long-aperture spectrometer, and LWLA $= 5.19$ x 10^{-9} sr for the long-wavelength, long-aperture spectrometer (Bohlin et al. 1980) for the normalization to unit steradian. The resulting nebular surface brightness values in the two UV bands are listed in Table 1.

For corresponding nebular scattered-light surface brightness values in the optical *B* (4410 Å) and *G* (5238 Å) bands, at the positions defined by the *IUE* pointing in the two nebulae, we referred to measurements published by Lai, Witt & Crawford (2017). We did not use data from the *R* (6464 Å) band, given that the presence of ERE in this band significantly contaminates the dust-scattered light in both nebulae. The data of Lai, Witt & Crawford (2017) (Table 2) are flux-calibrated intensities *S*, divided by the flux observed from gamma Cas, $F^{\star}$, in the two bands, listed together with the equatorial coordinates of the corresponding positions in the two nebulae. We interpolated and extrapolated from several of these Lai, Witt & Crawford (2017) positions closest to the *IUE* positions to arrive at best estimates for $\log(S/F^{\star})_B$ and $\log(S/F^{\star})_G$. The results are listed in Table 2, together with corresponding values for the two UV bands (see Section 2.4).

2.4 Far-UV flux from gamma Cas

We needed far-UV fluxes for gamma Cas for two purposes: One, to compute stellar-flux-normalized nebular surface brightness values $\log(S/F^{\star})$, two, to provide a basis from which to calculate the

Table 3. Far-IR photometric intensities at the tips of IC 63 and IC 59 adopted from Andrews et al. (2018).

	IC 63		IC 59	
λ (μm)	I_ν (MJy sr^{-1})	δI_ν	I_ν (MJy sr^{-1})	δI_ν
70	611.0	6.4	33.4	2.4
160	543.4	5.6	70.2	3.1
250	230.7	5.6	35.2	2.9
350	102.9	4.4	17.5	2.3
500	40.6	4.6	7.6	1.5

stellar UV fluxes in the energy range 6–13.6 eV incident on the surfaces of IC 59 and IC 63, once their distances from gamma Cas are determined.

For the first, we acquired low-resolution, large-aperture (10 arcmin x 20 arcmin) *IUE* gamma Cas spectra LWP13607 and SWP33895 from *MAST*. These spectra were flux-calibrated with the same absolute calibration as the nebular spectra, and any potential systematic errors in the calibration are expected to cancel when calculating the $(S/F^{\star})$ ratio. The average observed flux value for the 2600–2800 Å band was $<F^{\star}(2600-2800)> = 3.21$ x 10^{-9} erg cm^{-2} s^{-1} Å^{-1}, and for the 1750– 1900 Å band $<F^{\star}(1750-1900)> = 7.37$ x 10^{-9} erg cm^{-2} s^{-1} Å^{-1}.

For the wavelength-integrated UV flux in the 6–13.6 eV range, we combined the SWP33895 spectrum with the gamma Cas scattered-light spectrum obtained by the *Far Ultraviolet Spectroscopic Explorer (FUSE)* to extend the spectral coverage to the Lyman limit, as discussed by France et al. (2005) (Fig. 6). To obtain the far-UV flux, we binned the spectrum in 100 Å intervals and integrated it over the wavelength range corresponding to the energy range 6–13.6 eV. The observed band-integrated flux was found to be

$F^{\star}(6.0-13.6) = 1.28$ x 10^{-5} erg cm^{-2} s^{-1}. When corrected for interstellar extinction with $E(B - V) = 0.04$ mag with a CCM extinction curve with $R_V = 3.1$, $F^{\star}(6.0-13.6) = 1.91$ x 10^{-5} erg cm^{-2} s^{-1}, and when corrected for interstellar extinction for $E(B - V) = 0.08$ mag, $F^{\star}(6.0-13.6) = 2.93$ x 10^{-5} erg cm^{-2} s^{-1}.

2.5 Far-infrared intensities in IC 59 and IC 63

We adopted the *Herschel* Photodetector Array Camera and Spectrometer (PACS) intensities at 70 and 160 μm and The Spectral and Photometric Imaging REceiver *(SPIRE)* intensities at 250, 350, and 500 μm measured at the tips of IC 59 and IC 63 facing gamma Cas,
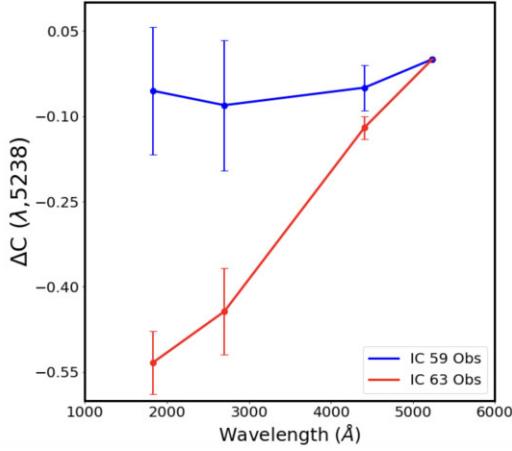
Figure 2. Nebula–Star colour differences for IC 59 and IC 63 relative to gamma Cas, normalized at $\lambda_2 = 5238$ Å.

as presented by Andrews et al. (2018). We have reproduced their values in Table 3.

2.6 ERE intensities in IC 59 and IC 63

Lai, Witt & Crawford (2017) mapped the ERE intensities across IC 59 and IC 63. They found maximum band-integrated ERE intensities of about 2.5 x 10^{-5} erg cm^{-2} s^{-1} sr^{-1} in IC 59 and 1.4 x 10^{-4} erg cm^{-2} s^{-1} sr^{-1} in IC 63. Spatially, the maximum ERE intensities were seen in the front regions of both nebulae facing gamma Cas. In IC 63, the stratification of different emission processes is more clearly discernible, in the sense that peak ERE emission occurs just behind the ionization front defined by the peak in H α emission but in front of most of the pure rotational band emission from H$_2$ (Fleming et al. 2010) and the emissions attributed to both ionized and neutral polycyclic aromatic hydrocarbon molecules (Lai, Witt & Crawford 2017). This supports an interpretation in which the ERE process traces environments dominated by photons in the 912–1100 Å wavelength range, where molecular hydrogen is either partially or totally dissociated. As long as the abundance of ERE carriers is sufficiently high relative to other absorbers of far-UV radiation, e.g. H$_2$, to absorb the bulk of the incident photons in the 912–1100 Å range, the ERE intensity can, therefore, serve as a measure of the density of the prevailing far-UV radiation field in environments dominated by atomic hydrogen.

3 ANALYSIS AND RESULTS

3.1 Nebula–star colour differences

Denoting the nebular surface brightness as S and the corresponding stellar flux as $F^\star$, and defining nebular and stellar colours, respectively as $\log(S_{\lambda_1}/S_{\lambda_2})$ and $\log(F^\star_{\lambda_1}/F^\star_{\lambda_2})$, we can write the colour difference (Witt 1985) as

$$\Delta C(\lambda_1, \lambda_2) =$$
$$\log(S_{\lambda_1}/S_{\lambda_2}) - \log(F^\star_{\lambda_1}/F^\star_{\lambda_2}) = \log(S_{\lambda_1}/F^\star_{\lambda_1}) - \log(S_{\lambda_2}/F^\star_{\lambda_2})$$
(1)

with $\lambda_1 < \lambda_2$. The wavelengths λ_1 and λ_2 are the effective wavelengths of any two bands involved in the colour measurement.

The nebula –gamma Cas colour differences for IC 59 and IC 63, normalized to the reference wavelength $\lambda_2 = 5238$ Å and calculated

from our observed values listed in Table 2, are shown in Fig. 2. The wavelength $\lambda_2 = 5238$ Å is the effective wavelength of the G-filter of Lai, Witt & Crawford (2017). We find that IC 63 is distinctly redder than gamma Cas in the UV-optical wavelength range, while the colour of IC 59 is nearly the same as that of gamma Cas. *Since there is no indication that the dust properties in the two nebulae are different from one another*, this difference is most readily explained by different effective angles under which the continuum light from gamma Cas is being scattered toward the observer.

Witt (1985) derived an approximate single-scattering expression for the colour difference $\Delta C(\lambda_1, \lambda_2)$ that includes a direct dependence on the scattering angle through the phase function of scattering. Modified for the case of an external illuminating star ($\tau_\star = 0$), this expression attains the form:

$$\Delta C(\lambda_1, \lambda_2) \approx$$
$$\log\left(\frac{a(\lambda_1) \times [1 - \exp(-\tau_0(\lambda_1))] \times \exp(-\tau_1(\lambda_1)) \times \Phi(\alpha, g(\lambda_1))}{a(\lambda_2) \times [1 - \exp(-\tau_0(\lambda_2))] \times \exp(-\tau_1(\lambda_2)) \times \Phi(\alpha, g(\lambda_2))}\right),$$
(2)

where $a(\lambda)$ is the wavelength-dependent dust albedo, $\tau_0(\lambda)$ is the line-of-sight optical depth through the nebula at the position of the observation, $\tau_1(\lambda)$ is the optical depth encountered by the star's light before reaching the position of observation, and $\Phi(\alpha, g(\lambda))$ is the scattering phase function for a scattering angle α and phase function asymmetry factor $g(\lambda)$. The scattering angle is defined as usual as the angle by which the scattered radiation is deflected relative to the incident beam of light. For the purpose of this study, we adopt the one-parameter Henyey & Greenstein (1941) (HG) phase function, with values for the dust albedo $a(\lambda)$ and the phase function asymmetry parameter $g(\lambda)$ based on empirically derived values from observations of the reflection nebulae NGC 7023 (Witt et al. 1992) and IC 435 (Calzetti et al. 1995).

As evident from Fig. 2, the largest difference in $\Delta C(\lambda_1, \lambda_2)$ between IC 59 and IC 63 occurs for ΔC (1825, 5238), suggesting that this value of the colour difference is most sensitive to differences in the effective scattering angles at the two nebulae. Using equation (2), we calculated possible values of ΔC (1825, 5238) for IC 59 as a function of the scattering angle, adopting $a(5238) = 0.55$, $g(5238) = 0.60$, $a(1825) = 0.65$, $g(1825) = 0.75$ (Witt et al. 1992; Calzetti et al. 1995). We estimated $\tau_0(5238) = 0.50$, given the relatively high transparency of IC 59 at the observed position, as judged by the number density of visible background stars. Both τ_0 and τ_1 were scaled to corresponding values at shorter wavelengths using a CCM extinction curve with $R_V = 3.7$ (Van De Putte et al. 2020). A comparison of predicted colour differences ΔC (1825, 5238) for a range $0.2 \le \tau_1(5238) \le 0.8$ with the value observed in IC 59 is shown in Fig. 3. The most likely effective scattering angle is found in the range $15° \le \alpha \le 50°$, consistent with a location of IC 59 in front of the plane of the sky containing gamma Cas.

We followed the same method to calculate the expected colour difference ΔC (1825, 5238) for IC 63, but using $\tau_0(5238) = 1.70$ instead, based on extinction measurements by Van De Putte et al. (2020) in the front parts of IC 63. In Fig. 4, we show a comparison of predicted colour differences as a function of the effective scattering angle α for a range of $0.4 \le \tau_1(5238) \le 0.8$ with the observed value in IC 63. This comparison suggests that the scattering in IC 63 occurs most likely with $\alpha > 90°$, placing IC 63 behind the plane of the sky containing gamma Cas, if the radial distance of IC 63 from gamma Cas is significantly in excess of the angular offset distance, which corresponds to about 1.0 pc.
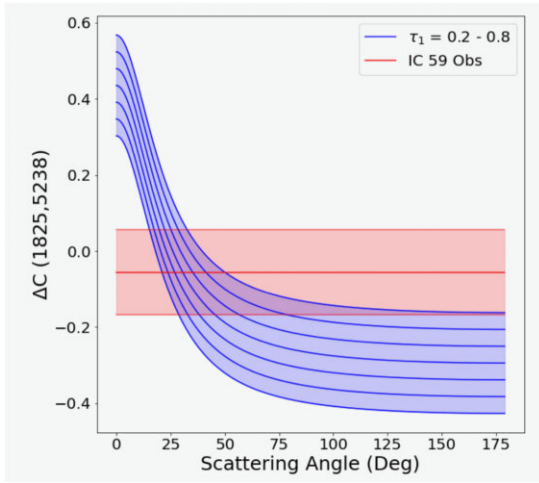
Figure 3. Predicted colour difference ΔC (1825, 5238), calculated with equation (2) for a set of values of $0.2 \leq \tau_1(5238) \leq 0.8$ (non-linear bands displayed from top to bottom) is compared with the observed colour difference ΔC (1825, 5238) in IC 59 (horizontal linear bands, with non-solid area representing measurement uncertainties). The most likely scattering angle found from the intersection of the most likely colour difference (horizontal lines) with the range of predicted colour differences (non-linear lines) is in the range $15° \leq \alpha \leq 50°$, consistent with a location of IC 59 in front of the plane of the sky containing gamma Cas.
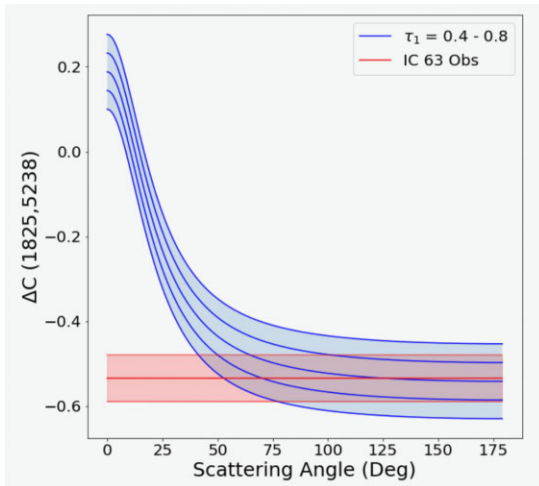

Figure 4. Predicted colour difference ΔC (1825, 5238), calculated with equation (2) for a set of values $0.4 \leq \tau_1(5238) \leq 0.8$ (non-linear bands displayed from top to bottom) is compared with the observed colour difference ΔC (1825, 5238) in IC 63 (horizontal linear bands, with non-solid area representing measurement uncertainties). The most likely scattering angle is $\alpha > 90°$, as found from the intersection of the most likely colour difference (horizontal lines) with the predicted colour difference (non-linear lines) for the most likely value of $\tau_1 = 0.6$.

3.2 Dust temperatures and radial distances

The equilibrium temperature of large dust grains in a radiation environment dominated by the luminosity $L_\star$ of a nearby star is a function of the radial distance from this star. Using the far-IR intensities (Table 3) observed at the tips of IC 59 and IC 63 by *Herschel* (Andrews et al. 2018) for the wavelength range $70\,\mu m \leq \lambda \leq 500\,\mu m$, we matched the far-IR SEDs with single-temperature
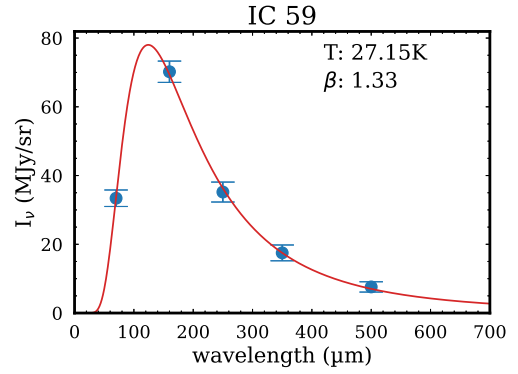

Figure 5. Modified blackbody fit to *Herschel* far-IR intensities over the 70–500 μm wavelength range for the tip of IC 59 facing gamma Cas. Data from Andrews et al. (2018).
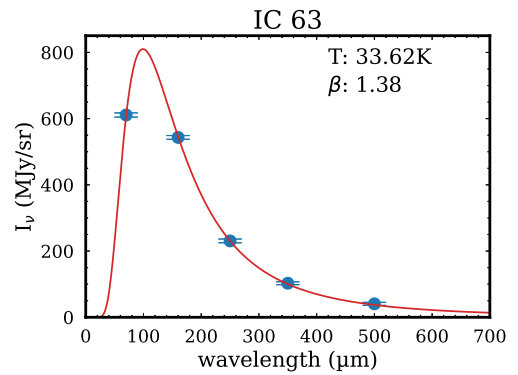

Figure 6. Modified blackbody fit to *Herschel* far-IR intensities over the 70–500 μm wavelength range for the tip of IC 63 facing gamma Cas. Data from Andrews et al. (2018).

modified blackbody fits, allowing both the dust temperature T_d and the spectral index β to be free parameters. The result for IC 59 is displayed in Fig. 5, that for IC 63 in Fig. 6. The best dust temperatures are T_d (IC 59) = 27.15 K and T_d (IC 63) = 33.62 K. These temperatures are well above the dust temperature found in the local diffuse interstellar medium of 20.4 ± 1.5 K (Bianchi et al. 2017) or even lower (Planck Collaboration XI 2014) and a clear indication of the dominance of the radiation from gamma Cas in the heating of the nebular dust. The results also indicate that IC 63 is significantly closer to gamma Cas than IC 59. The spectral indices β (IC 59) = 1.33 and β (IC 63) = 1.38 are consistent with a dust composition dominated by amorphous silicates and amorphous carbon (Ysard et al. 2019) and are well within the range of values encountered in interstellar dust in the Milky Way Galaxy (Dupac et al. 2003; Bianchi et al. 2017).

Krugel (2003), Urban, Evans & Doty (2009), and Draine (2011) developed detailed formalisms that relate the equilibrium temperature of large interstellar dust grains to the density of the incident radiation from a nearby star as a function of the radial distance r. The Krugel (2003) formalism, which is restricted to the case of $\beta = 2$, is not suitable for our data with β values of 1.33 and 1.37, found respectively for IC 59 and IC 63. The Draine (2011) formalism is developed for the more general case but with inputs involving the radiation field density rather than with explicit dependencies involving the star's luminosity and the radial distance from the star. We adopted the approach of Urban, Evans & Doty (2009) as the one

most readily applicable to our data, as it allows for general values of the spectral index β and provides a direct relation between the dust temperature and the star's radial distance r through the star's luminosity $L_\star$.

With a single star as the source of energy, the dust temperature is found as

$$T_{\mathrm{d}}(r) = K(\beta) \times [\frac{(L_\star/L_\odot)}{(r/1000\,\mathrm{AU})^2}]^{\frac{1}{4+\beta}}\,[K], \qquad (3)$$

where

$$K(\beta) = [\frac{3.89 \times 10^4}{\Gamma(4+\beta) \times \zeta(4+\beta)} \times \frac{Q(\mathrm{UV})}{Q(\nu_0)} \times (\frac{h\nu_0}{k})^\beta]^{\frac{1}{4+\beta}}. \qquad (4)$$

Here, β is the spectral index of the dust emissivity, GAMMA$(4+\beta)$ and $\zeta(4+\beta)$ are the Gamma and Riemann Zeta functions, $Q(\mathrm{UV})$ is the stellar-flux weighted absorption efficiency of the dust grains in the UV, while $\nu_0 = c/(125\,\mu\mathrm{m}) = 2.40 \times 10^{12}$ Hz.

Considering that dust in reflection nebulae typically resides in environments with densities two or three orders of magnitude higher than those in the diffuse interstellar medium, grain growth is expected. This seems confirmed by extinction measurements by Van De Putte et al. (2020) in IC 63, which revealed R_{V} values around 3.7 in the front part of the nebula. Thus, we regarded the Draine (2003) interstellar dust model for $R_{\mathrm{V}} = 4.0$ to be the closest representation of the dust in IC 59 and IC 63, and we used Draine (2003) as the source for $Q(\mathrm{UV})$ and $Q(125\,\mu\mathrm{m})$. In conjunction with the extinction-corrected $E(B - V) = 0.08$ far-UV flux distribution observed from gamma Cas, this dust model yields a ratio $Q(\mathrm{UV})/Q(\nu_0) = 2520$.

Then, using equation (4) with $\beta(\mathrm{IC}\,59) = 1.33$ (Fig. 5) and $\beta(\mathrm{IC}\,63) = 1.38$ (Fig. 6), we find $K(\mathrm{IC}\,59) = 50.33$ and $K(\mathrm{IC}\,63) = 49.93$.

Finally, using the best-fitting dust temperatures T_{d} (IC 59) = 27.15 K and T_{d} (IC 63) = 33.62 K, together with the adopted bolometric luminosity of gamma Cas, $L_\star = 27\,150\,\mathrm{L}_\odot$ (Sigut & Jones 2007), we find for the estimated radial distances from gamma Cas: $r(\mathrm{IC}\,59) = 4.15\,\mathrm{pc}$ and $r(\mathrm{IC}\,63) = 2.31\,\mathrm{pc}$. Combined with their offset distances of about 1.2 and 1.0 pc, respectively, and their locations relative to gamma Cas, these distances imply effective scattering angles of about $17°$ for IC 59 and about $154°$ for IC 63, which agree well with the range of scattering angles we found in Section 3.1.

3.3 Radial distance ratio from ERE constraints

Given that the ERE is excited by far-UV photons in the 10.5 eV < E < 13.6 eV energy range (Witt et al. 2006; Witt & Lai 2020) and taking that the emission is isotropic, we can use measured ERE intensities to estimate the density of the prevailing far-UV radiation field in the emitting environments. The maximum ERE surface brightness in IC 59 and IC 63 is observed in the front parts of both nebulae facing gamma Cas, i.e. regions exposed to the most direct and least attenuated far-UV flux from the star (Lai, Witt & Crawford 2017). The maximum ERE intensity in IC 59 of $I(\mathrm{ERE})_{\mathrm{IC}\,59} = 2.5 \times 10^{-5}\,\mathrm{erg\,cm^{-2}\,s^{-1}\,sr^{-1}}$ persist over a significant range of corresponding scattered light intensities, covering $1.5 \times 10^{-5}\,\mathrm{erg\,cm^{-2}\,s^{-1}\,sr^{-1}} \leq I(\mathrm{sca})_{\mathrm{IC}\,59} \leq 6.0 \times 10^{-5}\,\mathrm{erg\,cm^{-2}\,s^{-1}\,sr^{-1}}$. This is not unexpected for an optically thin nebula that receives its illumination from behind and where higher ERE intensities generated on its back surface are partially attenuated by the nebular dust.

The character of the ERE intensity distribution in IC 63 is very different in this respect. The maximum ERE intensity $I(\mathrm{ERE})_{\mathrm{IC}\,63} = 1.4 \times 10^{-4}\,\mathrm{erg\,cm^{-2}\,s^{-1}\,sr^{-1}}$ in IC 63 is observed in locations immediately behind the ionization front with a corresponding scattered light intensity of $I(\mathrm{sca})_{\mathrm{IC}\,63} \cong 3.5 \times 10^{-4}\,\mathrm{erg\,cm^{-2}\,s^{-1}\,sr^{-1}}$, only to drop precipitously with increasing offset distances from gamma Cas and decreasing scattered light intensities. This is consistent with illumination on the front side of the nebula as seen from Earth.

The ratio of the maximum ERE intensities $I(\mathrm{ERE})_{\mathrm{IC}\,63}/I(\mathrm{ERE})_{\mathrm{IC}\,59}$ = 5.60 suggest a ratio of the radial distances from gamma Cas r_{59}/r_{63} = $(I(\mathrm{ERE})_{\mathrm{IC}\,63}/I(\mathrm{ERE})_{\mathrm{IC}\,59})^{1/2}$ = 2.37. This is in fair agreement with the ratio $r_{59}/r_{63} = 1.80$ obtained from the dust temperatures. The distance ratio r_{59}/r_{63} inferred from the ratio of the ERE intensities appears larger because the observed ERE intensities in IC 59 are most likely reduced by self-attenuation within this nebula, given that it is being illuminated by gamma Cas from behind. By contrast, the ERE intensities in IC 63 are observed on the directly illuminated front side and are not affected by dust attenuation. If one accepts the distance ratio $r_{59}/r_{63} = 1.80$ derived from the dust temperatures as correct, the distance ratio derived from the ratio of the ERE intensities can be made to agree with this value by invoking self-attenuation of the ERE intensities in IC 59 by internal dust with an optical depth $\tau_{\mathrm{IC}\,59} = 0.54$. This optical depth is in good agreement with the values of τ_0 and τ_1 adopted for IC 59 to explain the observed colour difference ΔC (1825, 5238) in IC 59 (Section 2.1).

3.4 Radiation field densities in IC 63 and IC 59

Adopting the radial distances of the nebulae found from the analysis of their far-IR SEDs, $r_{\mathrm{IC}\,63} = 2.3\,\mathrm{pc}$ and $r_{\mathrm{IC}\,59} = 4.15\,\mathrm{pc}$, together with the revised distance to gamma Cas of (168 ± 4) pc and its extinction ($E(B - V) = 0.08$ mag) corrected far-UV flux $F_\star(6.0\text{–}13.6\,\mathrm{eV})$ = $2.93 \times 10^{-5}\,\mathrm{erg\,cm^{-2}\,s^{-1}}$, we can estimate the corresponding far-UV flux at the surfaces of the two nebulae facing gamma Cas. Compared to the extinction-corrected far-UV flux observed at Earth, the respective far-UV fluxes incident on the surfaces of the two nebulae are increased by the square of the ratio of the Earth – gamma Cas distance and the respective radial distances of the nebulae from gamma Cas. This results in far-UV fluxes incident on IC 59 of $4.80 \times 10^{-2}\,\mathrm{erg\,cm^{-2}\,s^{-1}}$ and incident on IC 63 of $1.55 \times 10^{-1}\,\mathrm{erg\,cm^{-2}\,s^{-1}}$. In Draine units of $2.7 \times 10^{-3}\,\mathrm{erg\,cm^{-2}\,s^{-1}}$, we find $G_0(\mathrm{IC}\,63) = 58$ and $G_0(\mathrm{IC}\,59) = 18$.

If the lower reddening of $E(B - V) = 0.04$ mag is accepted for gamma Cas, even lower values are found: $G_0(\mathrm{IC}\,63) = 38$ and $G_0(\mathrm{IC}\,59) = 12$.

Historically, far higher UV radiation field densities had been estimated, starting with G_0 (IC 63) = 650 (Jansen, van Dishoeck & Black 1994). The reduction to our current values is in part due to the actual distances of the nebulae from gamma Cas being two to four times larger than the offset distances in the sky that had initially been taken to be the actual distances. A second factor leading to the reduction was a change in the far-UV flux from gamma Cas seen at Earth. Jansen, van Dishoeck & Black (1994) adopted the result of Troy et al. (1975), who had observed gamma Cas during a 1971 sounding rocket flight. A flux of 1590 photons $\mathrm{cm^{-2}\,s^{-1}\,\mathring{A}^{-1}}$ was reported for the far-UV band 912–1075 Å, corresponding to about 3.3 $\times 10^{-8}\,\mathrm{erg\,cm^{-2}\,s^{-1}\,\mathring{A}^{-1}}$. The *IUE* – calibrated flux measured with *FUSE* in the same spectral region is about $1.4 \times 10^{-8}\,\mathrm{erg\,cm^{-2}\,s^{-1}}$ $\mathring{A}^{-1}$ (France et al. 2005), lower by about a factor 2.4. We adopted the latter for this work, because it was obtained with a vastly more sensitive and better calibrated instrument in Earth orbit compared to

the rocket experiment performed by Troy et al. (1975) three decades earlier.

4 DISCUSSION

We employed two distinctly different methods, combining UV/optical scattering data with far-IR flux measurements, to discern the spatial location and radial distances of the nebulae IC 59 and IC 63 relative to their common illuminating star gamma Cas.

The observed UV-optical colour differences between the nebulae and gamma Cas, coupled with the wavelength dependence of the scattering phase function asymmetry, yielded a clear signal placing IC 59 well in front of the plane of the sky containing the star, while indicating that the scattering in IC 63 most likely occurs at scattering angles $>90°$. Given that we relied on a single-scattering approximation, using the 1-parameter HG-phase function, we did not expect to find sufficiently precise scattering angles to infer actual star–nebula distances. This might be possible with a full multiple-scattering radiative transfer treatment with more appropriate phase functions (Baes, Camps & Kapoor 2022).

Instead, we used equilibrium dust temperatures determined with modified blackbody fits to the 70–500 μm far-IR intensities observed with *Herschel* to estimate the radial distances of the two nebulae from gamma Cas, given the previously known bolometric luminosity of the star. This, coupled with the result from the colour-difference approach, places IC 63 clearly behind the plane containing gamma Cas, at a radial distance of about 2.3 pc.

Our result for the location of IC 63 is in fair agreement with Andersson et al. (2013), who arrived, by totally different means, at the conclusion that IC 63 lies behind gamma Cas, with a radial distance of about 2 pc. Caputo et al. (2023) further amplified this conclusion, while also indicating the location for IC 59 in front of gamma Cas, at a radial distance of 4.5 pc, in reasonable agreement with our present result based on the observed dust temperature in IC 59.

We note that the estimate of the radial distances of the nebulae from gamma Cas through equations (3) and (4) is dependent on a dust model through the quantity $Q(\mathrm{UV})/(Q(\nu_0))$. We adopted a Draine (2003) dust model with $R_V = 4.0$ as one that most likely suits dust in comparatively dense interstellar cloud conditions found in IC 63 and IC 59. If we had used a Draine (2003) model with $R_V = 3.1$ instead, the ratio $Q(\mathrm{UV})/(Q(\nu_0))$ would increase due to the steeper extinction in the far-UV, taking on the value $Q(\mathrm{UV})/(Q(\nu_0)) = 2855$ with the far-UV flux distribution of gamma Cas. The parameters $K(\beta)$ would increase accordingly to $K(\mathrm{IC}\,59) = 51.10$ and $K(\mathrm{IC}\,63) = 50.72$, with corresponding increases in the radial distances to $r(\mathrm{IC}\,59) = 4.23$ pc and $r(\mathrm{IC}\,63) = 2.45$ pc. These increases of at most about 6 per cent over the $R_V = 4.0$ case indicate that the results of the distance estimation do not depend in a major way on the details of the adopted dust model.

Both methods used in our analysis assume that gamma Cas is an isotropic radiator. Not surprising for a Be star, gamma Cas is reported to rotate at (70 ± 10) per cent of its critical rotational velocity (Tycner et al. 2005). As a result, the three-dimensional shape of gamma Cas is expected to change from a spherical to a flattened, ellipsoidal configuration with a higher effective temperature in the polar regions compared to cooler equatorial zones. This implies that the far-UV radiative flux received at the surfaces of IC 59 and IC 63 may not only depend on their radial distances from gamma Cas but also on their spatial orientation with respect to the star's rotation axis. In addition,

the presence of a disc (Quirrenbach et al. 1997; Stee et al. 2012) is likely to induce additional changes in the stellar SED when seen from different directions. Given the level of approximation involved in our two approaches, we did not attempt to include either of these complications in our analysis.

With the new constraints on the relative locations and distances of IC 59 and IC 63 with respect to gamma Cas and the resulting more reliable estimates for the far-UV radiation densities prevailing in the two nebulae, we consider the gamma Cas–nebula system an ideal laboratory for the study of PDRs in the low-UV-radiation limit. The fact that both nebulae see radiation fields of likely very similar spectral shape but different densities offers opportunities for the testing of models not found in other frequently observed PDRs. Finally, at 168 ± 4 pc, IC 59 and IC 63 are the nearest PDRs, offering the opportunity for superior spatial resolution with modern instruments like *JWST*.

5 CONCLUSIONS

By combining an analysis of the nebula–star colour differences over the UV-optical wavelength range with an analysis of the far-IR SEDs of the dust in IC 59 and IC 63, we have shown that the 3D spatial arrangement of these two nebulae relative to their common illuminating star gamma Cas can be resolved. We conclude:

(1) IC 63 is located behind the plane of the sky containing gamma Cas. The tip of IC 63 closest to the star is located at a radial distance of about 2.3 pc from the star, with scattered light from the star redirected with a scattering angle of about 154°.

(2) IC 59 is in front of the plane of the sky containing gamma Cas. The radial distance from gamma Cas to the tip of IC 59 closest to the star is about 4.15 pc. The effective scattering angle for IC 59 is about 17°.

(3) The ratio of their radial distances is consistent with the ratio of the maximum ERE intensities observed in IC 59 and IC 63. This supports the utility of the ERE as a measure of the far-UV radiation density in each environment.

(4) The far-UV radiation densities in the two nebulae due to irradiation by gamma Cas, measured in Draine (1978) units, are estimated as $G_0 = 58$ and $G_0 = 38$ for IC 63 and $G_0 = 18$ and $G_0 = 12$ for IC 59, with the poorly constrained interstellar reddening values of gamma Cas of either of $E(B - V) = 0.08$ mag or $E(B - V) = 0.04$ mag being a major source of uncertainty.

(5) The reduction in the far-UV radiation density in IC 63 from $G_0 = 650$ used in earlier studies (Jansen, van Dishoeck & Black 1994) to the present values is a result, in part, of the radial distance being 2.3 times larger than the offset distance in the plane of the sky, and in part due to an overestimation of the far-UV flux from gamma Cas by Troy et al. (1975).

DATA AVAILABILITY

The data used in this article are available from public sources, as outlined in Section 2. Data generated during this work will be made available upon reasonable request to the corresponding author.

REFERENCES

Andersson B. G. et al., 2013, ApJ, 775, 84

Andrews H., Peeters E., Tielens A. G. G. M., Okada Y., 2018, A&A, 619, A170

Andriesse C. D., Piersma T. R., Witt A. N., 1977, A&A, 54, 841

Baes M., Camps P., Kapoor A. U., 2022, A&A, 659, A149

Bianchi S. et al., 2017, A&A, 597, A130

Blouin D., McCutcheon W. H., Dewdney P. E., Roger R. S., Purton C. R., Kester D., Bontekoe T. R., 1997, MNRAS, 287, 455

Bohlin R. C., Holm A. V., Savage B. D., Snijders M. A. J., Sparks W. M., 1980, A&A, 85, 1

Bonne L. et al., 2023, AJ, 165, 243

Calzetti D., Bohlin R. C., Gordon K. D., Witt A. N., Bianchi L., 1995, ApJ, 446, L97

Caputo M., Soam A., Andersson B. G., Dennis R., Chambers E., Güsten R., Knee L. B. G., Stutzki J., 2023, ApJ, 950, 140

Cardelli J. A., Clayton G. C., Mathis J. S., 1989, ApJ, 345, 245 (CCM)

Chen X. et al., 2021, ApJ, 922, 183

Draine B. T., 1978, ApJS, 36, 595

Draine B. T., 2003, ApJ, 598, 1017

Draine B. T., 2011, Physics of the Interstellar and Intergalactic Medium Section 24. Princeton Univ. Press, Princeton, NJ

Dupac X. et al., 2003, A&A, 404, L11

Fleming B., France K., Lupu R. E., McCandliss S. R., 2010, ApJ, 725, 159

France K., Andersson B. G., McCandliss S. R., Feldman P. D., 2005, ApJ, 628, 750

Habart E., Boulanger F., Verstraete L., Walmsley C. M., Pineau des Forêts G., 2004, A&A, 414, 531

Habing H. J., 1968, Bull. Astron. Inst. Netherlands, 19, 421

Henry G. W., Smith M. A., 2012, ApJ, 760, 10

Henyey L. G., Greenstein J. L., 1941, ApJ, 93, 70

Hurwitz M. et al., 1998, ApJ, 500, L61

Jansen D. J., van Dishoeck E. F., Black J. H., 1994, A&A, 282, 605

Jansen D. J., van Dishoeck E. F., Black J. H., Spaans M., Sosin C., 1995, A&A, 302, 223

Jansen D. J., van Dishoeck E. F., Keene J., Boreiko R. T., Betz A. L., 1996, A&A, 309, 899

Kaplan K. F., Dinerstein H. L., Kim H., Jaffe D. T., 2021, ApJ, 919, 27

Karr J. L., Noriega-Crespo A., Martin P. G., 2005, AJ, 129, 954

Klement R. et al., 2017, A&A, 601, A74

Krugel E., 2003, The Physics of Interstellar Dust. The Insitute of Physics, Bristol, UK

Lai T. S. Y., Witt A. N., Crawford K., 2017, MNRAS, 469, 4933

Miao J., Sugitani K., White G. J., Nelson R. P., 2010, ApJ, 717, 658

Nikolov Y. M., Zamanov R. K., Stoyanov K. A., Martí J., 2017, Bulg. Astron. J., 27, 10

Perryman M. A. C. et al., 1997, A&A, 323, L49

Planck Collaboration XI, 2014, A&A, 571, A11

Quirrenbach A. et al., 1997, ApJ, 479, 477

Schild R., 1983, A&A, 120, 223

Schirmer T., Ysard N., Habart E., Jones A. P., Abergel A., Verstraete L., 2022, A&A, 666, A49

Sigut T. A. A., Jones C. E., 2007, ApJ, 668, 481

Smith T. L., Witt A. N., 2002, ApJ, 565, 304

Soam A., Maheswar G., Lee C. W., Neha S., Andersson B. G., 2017, MNRAS, 465, 559

Soam A., Andersson B. G., Karoly J., DeWitt C., Richter M., 2021, ApJ, 923, 107

Stee P. et al., 2012, A&A, 545, A59

Sternberg A., 1989, ApJ, 347, 863

Thi W. F., van Dishoeck E. F., Bell T., Viti S., Black J., 2009, MNRAS, 400, 622

Troy B. E. J., Johnson C. Y., Young J. M., Holmes J. C., 1975, ApJ, 195, 643

Tycner C. et al., 2005, ApJ, 624, 359

Urban A., Evans Neal J. I., Doty S. D., 2009, ApJ, 698, 1341

Van De Putte D., Gordon K. D., Roman-Duval J., Williams B. F., Baes M., Tchernyshyov K., Lawton B. L., Arab H., 2020, ApJ, 888, 22

van Leeuwen F., 2007, A&A, 474, 653

Witt A. N., 1977, PASP, 89, 750

Witt A. N., 1985, ApJ, 294, 216

Witt A. N., Lai T. S. Y., 2020, Ap&SS, 365, 58

Witt A. N., Stecher T. P., Boroson T. A., Bohlin R. C., 1989, ApJ, 336, L21

Witt A. N., Petersohn J. K., Bohlin R. C., O'Connell R. W., Roberts M. S., Smith A. M., Stecher T. P., 1992, ApJ, 395, L5

Witt A. N., Gordon K. D., Vijh U. P., Sell P. H., Smith T. L., Xie R.-H., 2006, ApJ, 636, 303

Ysard N., Koehler M., Jimenez-Serra I., Jones A. P., Verstraete L., 2019, A&A, 631, A88

This paper has been typeset from a TeX/LaTeX file prepared by the author.